Measurement of the Target Asymmetry of η and π^0 Photoproduction on the Proton

A. Bock,*,† G. Anton,* W. Beulertz,* Chr. Bradtke, H. Dutz, R. Gehring,‡ S. Goertz,‡ K. Helbing,* J. Hey,* W. Meyer,‡ M. Plückthun, G. Reicherz,‡ and L. Sözüer*

Physikalisches Institut der Universität Bonn, Nußallee 12, D-53115 Bonn, Germany

M. Breuer, J. P. Didelez, and P. Hoffmann-Rothe

IN2P3, Institut de Physique Nucleaire, 91406 Orsay, France

(Received 4 August 1997)

At the tagged photon facility PHOENICS at the Bonn accelerator ELSA a measurement of the target asymmetry of the reaction $\gamma p \rightarrow p\eta$ from threshold to 1150 MeV has been performed. Simultaneously the reaction $\gamma p \rightarrow p\pi^0$ has been measured in the first resonance region. Results are presented for both reactions. The target asymmetry data are suited to put considerable constraints on the model parameters used for the theoretical description of meson photoproduction. [S0031-9007(98)06654-X]

PACS numbers: 25.20.Lj, 13.60.Le, 14.20.Gk, 24.70.+s

Meson production from nucleons is a major tool for the investigation of nucleon resonances. The technical development of tagged photon beams at high duty cycle accelerators has initiated a series of high precision experiments dedicated to the study of meson photoproduction. A lot of data have been obtained for the production of pions, and theoretical models have been developed which describe the data by resonance excitation and Born terms. The application of these models to another meson provides a good test of the assumptions and the predictive power. Moreover, a model which covers different meson production channels leads to a consistent picture of meson nucleon dynamics.

In the case of η photoproduction some special aspects occur. The eta has isospin $I = 0$ and, accordingly, only $I = 1/2$ nucleon resonances N^* can be excited. Further, a resonance state has several decay channels with different decay probabilities. This offers the possibility that a resonance state is almost hidden in pion production while it is rather prominent in eta photoproduction, as is the case for the $S_{11}(1535)$ [1]. The dominance of the $S_{11}(1535)$ in the reaction $\gamma N \rightarrow \eta N$ has been seen in the total and in the differential cross section in the threshold region [2]. Consequently, the eta channel is well suited for the precise determination of the $S_{11}(1535)$ resonance parameters. The contribution of weakly excited resonances to the cross section is only small and is hard to disentangle [3]. One example is the resonance $D_{13}(1520)$ which might be the source of an observed small anisotropy of the $\gamma p \rightarrow \eta p$ cross section [1]. Here, polarization observables offer an enhanced sensitivity because they contain bilinear products of partial waves, respectively, of multipoles. For the $D_{13}(1520)$, an observable such as the target asymmetry, which contains an interference of the strong $S_{11}(1535)$ with the weak $D_{13}(1520)$, is very advantageous.

The experiment presented here is part of the extended program of η photoproduction that has been carried out at the PHOENICS facility at the Bonn accelerator ELSA. It included measurements of differential and total cross sections on the proton, neutron, deuteron, and nitrogen over a wide kinematic range [4,5]. In this framework the reaction $\gamma p \rightarrow p\eta$ has been investigated using a polarized proton target.

The electron beam extracted from ELSA was used to produce a photon beam by bremsstrahlung at a thin radiator. The tagging system in the PHOENICS area [6] determined the energy and flux of the photons in the energy range $E_\gamma = 250-1150$ MeV. The energy resolution ranges from $\sigma_{E_\gamma} = 2.4$ to 4.4 MeV. The flux of photons impinging on the target was determined by additional measurements with a total absorbing lead glass detector positioned in the primary photon beam. The difference between the number of tagged electrons and the number of photons arises from nonbremsstrahlung events at the tagging target and collimation of the photon beam.

The Bonn frozen spin target provided polarized protons with a maximum polarization of 85% achieved by means of dynamic nuclear polarization [7]. During data acquisition these polarization values were maintained with the low field (0.35 T) of a superconducting coil located inside the refrigerator [8]. This new concept was introduced to meet the requirements of the detector arrangement and to minimize the influence on low energy particles. Butanol (C_4H_9OH) was chosen as target material because of its reasonable fraction of polarizable protons compared to the completely nonpolarizable background nuclei (C_4O).

In order to reduce systematic errors the direction of the target spins was inverted every two days. The polarization was measured at the beginning and end of each data acquisition cycle and was monitored in between by the target temperature which determines the exponential decrease of the polarization. The measurement followed the standard nuclear magnetic resonance technique. The absolute values were calibrated by the so-called thermal equilibrium method. The relative polarization errors resulting from this calibration and small cusps of the target temperature vary between 2% and 4%.

 0031-9007/98/81(3)/534(4)$15.00 © 1998 The American Physical Society

The reaction was identified by detecting the η decay photons in the neutral meson spectrometer SPES$\varnothing$ 2π while the recoil protons' four momentum was determined with the large angle detector PHOENICS (see Fig. 1).

The SPES$\varnothing$ 2π detector [9] consists of an arrangement of eight lead glass bars (8 cm thick) that directly surround the target in a cylindrical geometry. Each detector covers an angular range of 30° in the horizontal and ±70° in the vertical plane and is equipped with photomultiplier tubes at both ends. Impinging photons convert into electromagnetic showers which are detected via the produced Čerenkov light. In order to suppress charged particles originating from background processes a plastic scintillator is positioned in front of each lead glass module. The trigger condition of the detector required the simultaneous detection of two photons on either side of the detector. This is mainly a kinematic selection favoring the η decay into two photons. At the same time the acceptance for pion photoproduction products is strongly reduced with the exception of the Δ-resonance region, where the detection probability reaches moderate values. The acceptance leakage in the forward direction (±30° in the horizontal plane) was exploited to detect the recoil protons with the PHOENICS scintillation counters [traditionally called proton (PC) and neutron counters (NC)] [10]. Their position with respect to the target was optimized to have similar acceptance and a good time-of-flight resolution in spite of different dimensions.

The complete four momentum of the recoil proton was determined by measuring its time of flight and its impact position on the detector. The combined information of deposited energy and time of flight allowed particle identification which was used to separate obvious background events with deuterons and electrons in the final state. Furthermore, a χ^2 minimization based on the code MINUIT (CERN) was performed to reject the remaining background. Assuming a free proton in the initial and final state, the reaction is kinematically overdetermined. We used the measured quantities of the proton and their experimental errors for this kinematic fit. The errors included the experimental time and angle resolution as well as smearing effects due to energy loss and multiple scattering. These effects were investigated with the help of a Monte Carlo simulation of the complete experimental setup based on the GEANT3 code. Background events were removed by means of a kinematic fit as a first step followed by the subtraction of the carbon data. This procedure is outlined in more detail below.

Depending on the primary photon energy, either π^0 production (for $E_\gamma < 700$ MeV) or η production was assumed as the nominal process for the fit. For the background elimination we did not refer to the χ^2 distribution itself but to the equivalent probability distribution $P(\chi^2)$. According to its definition, $P(\bar{\chi}^2) = \int_{\bar{\chi}^2}^{\infty} \chi^2(x,n)dx$, the probability distribution leads to a flat distribution for "good" events following the supposed χ^2 distribution. This method simplifies the separation of background events because those lead to a deviation from the flat distribution at low probability values. Their contribution could, consequently, be removed by a cut at $P(\chi^2) = 0.2$ (see Fig. 2). This value presented a compromise between good background suppression and small statistical errors. We checked the method by varying the cutoff value of the probability distribution. In this procedure only small variations of the results occurred that were fully compatible with the statistical uncertainty.

The background arises mainly from processes off bound nucleons inside the target and the surrounding materials. We performed additional measurements with a carbon target in order to determine these contributions. The carbon data were analyzed in an identical way and, after being normalized to the luminosity, they were used to determine the dilution factor (see below). The yield of protons fulfilling the kinematic cut was then extracted from missing mass spectra. Figure 3 shows the missing mass distribution obtained with the butanol and the carbon target before and after the kinematic cut. The right figure represents the relevant signal to determine the target asymmetry.

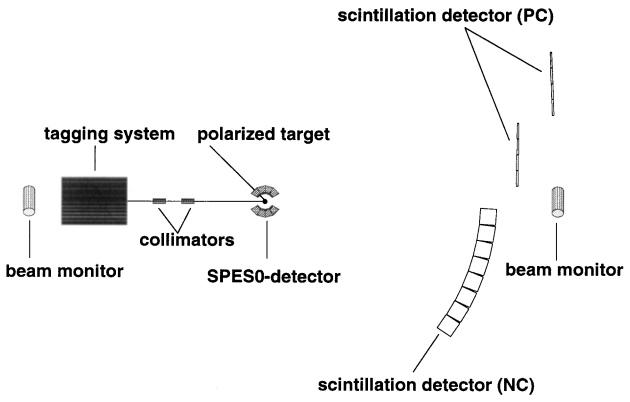

FIG. 1. Top view of the experimental setup.

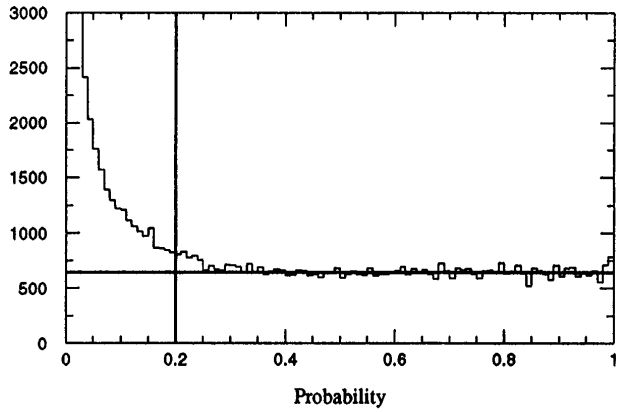

FIG. 2. Probability distribution of the reaction $\gamma p \to p\eta$. Events of the nominal process have a flat distribution while background events lead to a rise at small values. The vertical line indicates the cutoff value for background events.

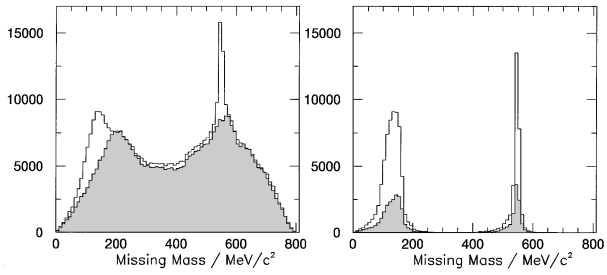

FIG. 3. Missing mass distributions for butanol and carbon (shadowed) before (left) and after (right) the kinematic fit.

The determination of the target asymmetry T off the proton follows its definition in the differential cross section for polarized nucleons σ_p:

$$\sigma_p = \sigma_0\{1 + p_y T \sin\phi\}, \tag{1}$$

where σ_0 is the unpolarized differential cross section off the free proton and p_y designates the polarization value of the target. The direction of the target spins has an angle ϕ to the plane defined by the vector of the primary photon and the produced meson ($\vec{k} \times \vec{q}$). Introducing the dilution factor $\kappa = \sigma_0/\sigma_{\text{butanol}}$, Eq. (1) can be extended to composed targets such as butanol. One derives the following relation for T in terms of the count rates belonging to different polarization states $(N_\uparrow, N_\downarrow)$:

$$T = \frac{1}{\kappa} \frac{N_\uparrow - N_\downarrow}{p_\downarrow N_\uparrow \sin\phi + p_\uparrow N_\downarrow \sin\phi}. \tag{2}$$

Because of the geometry of the detecting system the target asymmetry could be determined in two independent ways. As usual, the target polarization was inverted regularly. Apart from that, the geometric arrangement of the PHOENICS detectors on the right-hand side as well as on the left-hand side of the primary photon beam allowed a simultaneous detection of protons corresponding to $N_\uparrow$ in one detector group while the other one accepted those corresponding to $N_\downarrow$. The data were independently analyzed for the two types of detectors which reduced the systematical error. Both methods show a good agreement and the weighted average of both is presented here.

As a cross check, the same analysis was applied to the reaction $\gamma p \to p\pi^0$ in the Δ-resonance region. At meson production angles around 90° there is an overlap with existing data of two different measurements [11,12].

The results for this channel, only an example is presented in Fig. 4, are in good agreement with older ones (in total, seven of eight data points that are directly comparable overlap within 1σ) and, furthermore, extend to larger pion angles. The error bars include statistical as well as systematical errors. The latter are dominated by the uncertainty of the target polarization and the luminosity. The agreement of our results and the older data present a further consistency check of our analysis procedure.

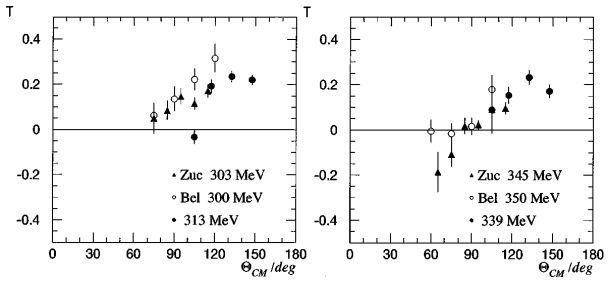

FIG. 4. Results for $\gamma p \to p\pi^0$.

The data of the channel $\gamma p \to p\eta$ are shown for some photon energies in Fig. 5 and are summarized in Table I. Near threshold the angular distribution has a clear structure, i.e., a change in sign at $\Theta_{\text{CM}} = 90°$. This behavior can be understood qualitatively by the following simple consideration. The expansion of the target asymmetry into leading multipoles ($J_{\eta N} \leq 2$) yields

$$T = -\frac{1}{\sigma_0} 3 \sin\theta \cos\theta \,\text{Im}\,[E_{0+}^*(E_{2-} + M_{2-})].$$

The interference of the dominant E_{0+} multipole [corresponding to the $S_{11}(1535)$] with the D-wave multipoles E_{2-} and M_{2-}, which contain the contribution of the $D_{13}(1520)$, leads to an angular structure proportional to $\sin\theta\cos\theta$. This behavior is apparently contained in the data.

More sophisticated theoretical analyses of meson photoproduction are based mainly on isobar models [13] or on effective Lagrangian approaches [3,14]. Resonance excitation is usually modeled by a Breit-Wigner function while the nonresonant terms are treated either by a weak energy dependent function or by the explicit evaluation of Born terms and vector meson exchange terms. The calculation of the nonresonant terms contains model

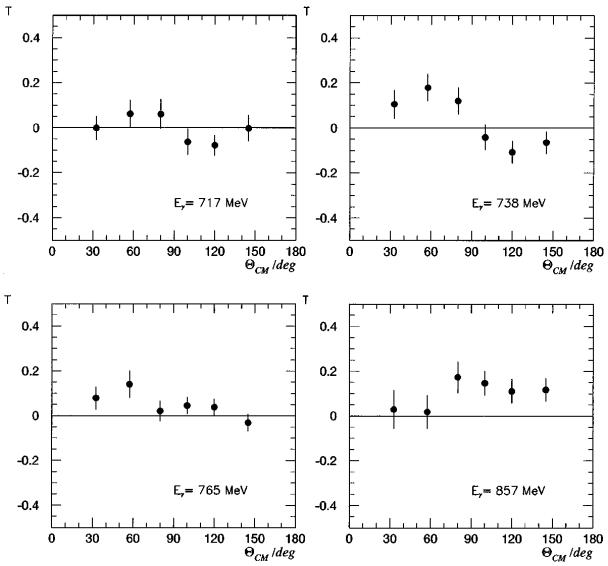

FIG. 5. Results for $\gamma p \to p\eta$.

TABLE I. Results of $\gamma p \to p\eta$.

E_γ [MeV]	T	ΔT	T	ΔT
	$\Theta_{CM} = 33 \pm 12°$		$\Theta_{CM} = 58 \pm 12°$	
717 ± 8	-0.002	0.053	0.061	0.059
738 ± 12	0.105	0.064	0.179	0.066
765 ± 14	0.078	0.051	0.140	0.061
790 ± 11	0.030	0.057	0.072	0.048
820 ± 14	-0.020	0.064	0.025	0.046
857 ± 18	0.029	0.087	0.018	0.075
895 ± 17	0.155	0.217	0.011	0.179
	$\Theta_{CM} = 80 \pm 10°$		$\Theta_{CM} = 100 \pm 10°$	
717 ± 8	0.060	0.066	-0.063	0.058
738 ± 12	0.120	0.060	-0.042	0.056
765 ± 14	0.021	0.045	-0.015	0.048
790 ± 11	-0.015	0.048	0.080	0.042
820 ± 14	0.125	0.051	0.063	0.040
857 ± 18	0.173	0.070	0.146	0.055
895 ± 17	0.203	0.094	0.127	0.065
947 ± 32	0.098	0.120	0.048	0.059
	$\Theta_{CM} = 120 \pm 10°$		$\Theta_{CM} = 145 \pm 15°$	
717 ± 8	-0.077	0.046	-0.002	0.059
738 ± 12	-0.107	0.050	-0.065	0.050
765 ± 14	0.038	0.037	-0.031	0.039
790 ± 11	-0.015	0.040	-0.020	0.044
820 ± 14	0.041	0.041	0.052	0.040
857 ± 18	0.111	0.054	0.117	0.052
895 ± 17	0.023	0.056	0.129	0.052
947 ± 32	0.145	0.059	0.089	0.046
1023 ± 40	0.140	0.059	0.102	0.046
1105 ± 40	0.086	0.066	0.167	0.093

dependencies concerning pseudoscalar and pseudovector coupling strength and vertex form factors.

The analysis of the differential cross section indicates a significant contribution of the $D_{13}(1520)$ resonance [15], but the unpolarized data do not contain sufficient information to determine its strength [14].

The effective Lagrangian model of [16] that gives the best agreement with these cross section data predicts a negative polarized target asymmetry in the $N^*(1535)$ excitation region, which is in contradiction to our data. However, attenuating the role of $N^*(1520)$ in this approach one can get a combined fit of the Mainz differential cross section data [15] and our results [17].

With increasing photon energy the asymmetry values remain small which is in contradiction to model predictions that suggest an increasing asymmetry at higher energies [3,16]. This situation is shown for Ref. [3] in Fig. 6. Although their approach also contains the data of [15], the prediction fails. More theoretical work is needed to extract precisely the resonance parameters. The ongoing measurements of the photon asymmetry of eta photoproduction at GRAAL (Grenoble) will deliver further constraints.

In conclusion, the results of our experiment represent the extension of the existing data to a new polarization observable in this energy region. The target asymmetry can be used to test the predictions of theoretical models, especially concerning the excitation of D-wave resonances. Up to now, existing model calculations fail to give a consistent description of the data.

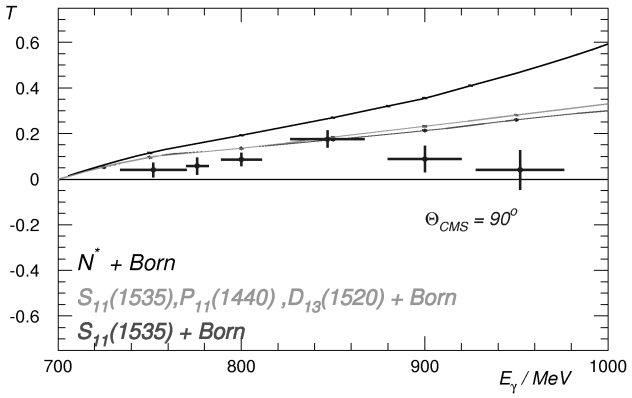

FIG. 6. Comparison of our data and the prediction from Ref. [3]. The curves consider contributions of different resonances.

*Present address: Physikalisches Institut der Universität Erlangen-Nürnberg, Erwin-Rommel-Str. 1, D-91058 Erlangen.
†Email address: bock@phop4.physik.uni-bonn.de
‡Present address: Physikalisches Institut der Ruhr-Universität Bochum, Universitätsstr. 150, D-44780 Bochum.

[1] L. Tiator, C. Bennhold, and S. S. Kamalov, Nucl. Phys. **A580**, 455 (1994).
[2] M. Benmerrouche, N. C. Mukhopadhyay, and J. F. Zang, Phys. Rev. D **51**, 3237 (1995).
[3] G. Knöchlein, D. Drechsel, and L. Tiator, Z. Phys. A **352**, 327 (1995); G. Knöchlein, diploma thesis, University of Mainz (1995).
[4] P. Hoffmann-Rothe *et al.*, Phys. Rev. Lett. **78**, 4697 (1997).
[5] J. Hey *et al.* (to be published).
[6] P. Detemple *et al.*, Nucl. Instrum. Methods Phys. Res., Sect. A **321**, 479 (1992).
[7] H. Dutz *et al.*, Nucl. Instrum. Methods Phys. Res., Sect. A **340**, 272 (1994).
[8] R. Gehring, Ph.D. thesis, University of Bonn, 1996.
[9] G. Rappenecker *et al.*, Nucl. Phys. **A590**, 763 (1995).
[10] K. Büchler *et al.*, Nucl. Phys. **A570**, 580 (1994).
[11] A. Belyaev *et al.*, Sov. J. Nucl. Phys. **35**, 401 (1982).
[12] B. Zucht, Ph.D. thesis, University of Bonn (to be published).
[13] H. R. Hicks *et al.*, Phys. Rev. D **7**, 2614 (1973).
[14] N. C. Mukhopadhyay, J.-F. Zhang, and M. Benmerrouche, Phys. Rev. Lett. **75**, 3022 (1995).
[15] B. Krusche *et al.*, Phys. Rev. Lett. **74**, 3736 (1995).
[16] N. C. Mukhopadhyay, J.-F. Zhang, and M. Benmerrouche, Phys. Lett. B **364**, 1 (1995).
[17] N. C. Mukhopadhyay and N. Mathur (to be published).